

TiO₂/Ferroelectric Heterostructures as Dynamic Polarization-Promoted Catalysts for Photochemical and Electrochemical Oxidation of Water

Jun Hee Lee* and Annabella Selloni

Department of Chemistry, Princeton University, Princeton, New Jersey 08544, USA

(Received 22 November 2013; revised manuscript received 18 February 2014; published 13 May 2014)

Using first-principles density functional theory calculations, we explore the chemical activity of epitaxial heterostructures of TiO₂ anatase on strained polar SrTiO₃ films focusing on the oxygen evolution reaction (OER), the bottleneck of water splitting. Our results show that the reactivity of the TiO₂ surface is tuned by electric dipoles dynamically induced by the adsorbed species during the intermediate steps of the reaction while the initial and final steps remain unaffected. Compared to the OER on unsupported TiO₂, the combined effects of the dynamically induced dipoles and epitaxial strain strongly reduce rate-limiting thermodynamic barriers and significantly improve the efficiency of the reaction.

DOI: 10.1103/PhysRevLett.112.196102

PACS numbers: 82.45.Jn, 82.45.Un, 82.50.-m, 77.55.fp

Titanium dioxide (TiO₂) is widely used in photocatalysis and solar energy conversion due to its many favorable properties, like stability against photocorrosion and proper band alignment relative to the water redox potentials [1–3]. However, the efficiency of TiO₂ is notoriously low, and efforts at improving it through modifications such as doping [4] or synthesis of (nano)crystals exposing highly reactive facets [5] have encountered only limited success. Among the possible alternatives to TiO₂, polar materials have recently attracted significant interest because their surface dipoles can react easily with charged species and supply built-in electric potentials to increase the carrier mobility [6,7]. However, control of the surface reactivity of these materials is difficult [8], e.g., because exposed surface dipoles often cause undesired atomic or electronic reconstructions and unexpected adsorption of charged species which can interfere with the reaction of interest [9–11]. Less well known than TiO₂ and polar semiconductors are heterostructures composed of stable TiO₂ thin films supported by a ferroelectric substrate [12,13]. Experimental studies have shown that the surface reactivity of TiO₂ is directly influenced and improved by the underlying ferroelectric domain structure, an effect that has been attributed to the combined efficient absorption and charge separation in the ferroelectric substrate and transport across the TiO₂/substrate interface [12,13]. Despite some encouraging results [13,14], however, the interest in such TiO₂/ferroelectric heterostructures has remained limited. In particular, their physical properties are largely unexplored and an atomic-scale understanding of their reactivity is missing.

We present here a first-principles density functional theory (DFT) study of TiO₂/ferroelectric heterostructures, which provides evidence that these composite materials can have a substantially enhanced reactivity relative to TiO₂. We focus on model heterostructures composed of a TiO₂ (001) film of anatase (the TiO₂ polymorph most efficient

for photocatalysis [15]) supported by a nearly ferroelectric SrTiO₃ (STO) substrate that can easily acquire a macroscopic polarization in the presence of an external perturbation such as electric field and epitaxial strain [16,17]. These structures are denoted TiO₂/STO in the following. Anatase has a small lattice mismatch with STO, so it can be grown on STO epitaxially [18]. While defects, e.g., oxygen vacancies, are almost invariably present in the experimentally prepared materials, it is reasonable to restrict to ideal, defect-free heterostructures in this first study. We probe the surface reactivity by investigating the oxygen evolution reaction (OER), which is known to be the bottleneck of water splitting [19,20], and show that the activity is directly related to the changes of the dynamically induced polarization in the supported TiO₂ film during the reaction. By varying the strain and thickness of the STO substrate, we further show that the strain and the induced dipole can be synergistically tuned to optimize the surface reactivity for the reaction of interest.

Our study is based on spin-polarized DFT calculations in the generalized gradient approximation (GGA) of Perdew-Burke-Ernzerhof (PBE) [21] and the plane-wave-pseudopotential scheme as implemented in the PWSCF code of the QUANTUM ESPRESSO package [22]. Selected calculations using the DFT + *U* approach [23] are discussed below. We consider TiO₂/STO model heterostructures composed of four anatase TiO₂(001) layers on top of seven (four TiO₂ and three SrO) layers of STO, with the two bottom layers (corresponding to one unit cell) fixed at the atomic positions of strained polar bulk STO (Fig. 1). As usual, below STO three Pt(001) layers are included to screen the dipole moments of STO [24,25]. We use a (2 × 1) surface cell, with a 2 × 4 × 1 mesh to sample *k* space. Consecutive slabs are separated by a ~ 10 Å vacuum with a dipole correction layer. All structures are relaxed until residual forces are smaller than 7.35 × 10⁻⁴ au. With this setup, the computed in-plane lattice constants of TiO₂

anatase and STO are 3.786 and 3.938 Å (+4.0% relative to anatase) and corresponding experimental values are 3.782 and 3.905 Å (+3.3%). The induced polarization in TiO_2 is determined from the average cation-anion displacements ($\Delta z = z_{\text{Ti}} - z_{\text{O}}$) multiplied by the relevant effective charges (details in Supplemental Material [26]). We approximate the charges of TiO_2/STO [27] by the effective charges of strained bulk TiO_2 that we calculate using the Berry-phase method.[28]

In Fig. 1, the effects of the STO polarization on the band edges and work function of TiO_2 are illustrated for two heterostructures, $(\text{TiO}_2/\text{STO})_{\pm}$, with opposite polarizations of the bottom STO layers of $\pm 0.8 \text{ C/m}^2$, which result from a STO compressive strain of 4%. The electrostatic potential energy profiles, Fig. 1(B), and densities of states (DOS), Fig. 1(C), show that there is a substantial

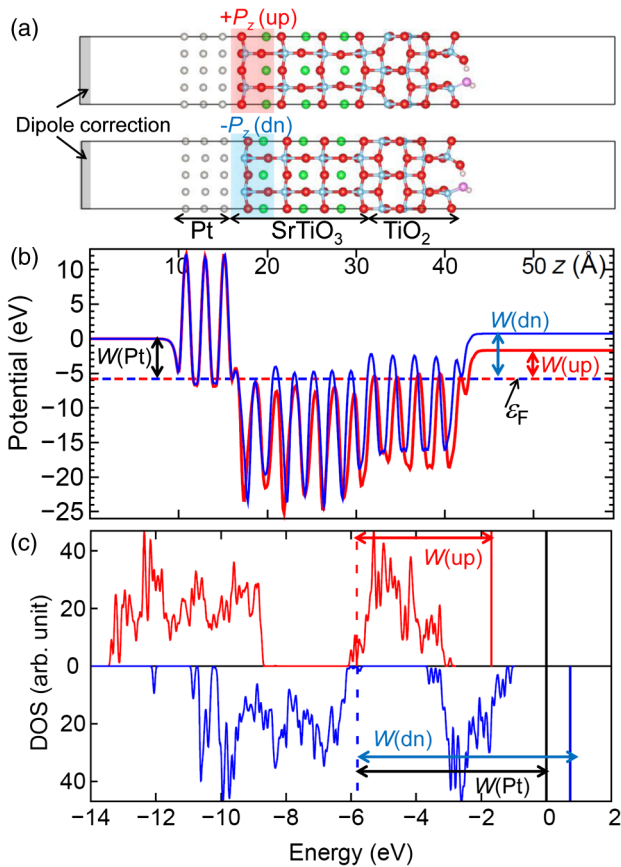


FIG. 1 (color online). (a) Calculated geometries of TiO_2/STO heterostructures with the atomic positions in the bottom STO layers fixed to those of positively (red) or negatively (blue) polarized bulk STO compressively strained to the lattice constant of bulk TiO_2 . The exposed anatase (001) surface is stabilized by a half monolayer of adsorbed water.[20] O, Ti, Sr, Pt, and H atoms are represented by red, cyan, green, gray, and white balls, respectively. (b) Electrostatic potential energy profiles, Fermi levels ϵ_F , and work functions of the Pt, $W(\text{Pt})$, and TiO_2 , $W(\text{up/dn})$, surfaces. (c) Electronic density of states of the TiO_2 films. Vertical lines correspond to the Fermi levels (dashed lines) and vacuum levels for the Pt (black) and TiO_2 (red/blue) surfaces.

difference, $\sim 2.5 \text{ eV}$, between the work-functions of the two TiO_2 surfaces and a nearly rigid shift of similar magnitude between the DOS curves of the two heterostructures. Analysis of the layer resolved DOS (Fig. S2-1 in the Supplemental Material [26]) further shows that the shift is similar for the different TiO_2 layers up to the top surface. This may be due to the relatively low static dielectric constant of anatase along the [001] direction ($\epsilon_{zz} = 22.7$ [29]).

OER free energy profiles on TiO_2/STO are calculated following a simple, yet effective scheme [30] that has been recently applied to various unsupported TiO_2 rutile [19,30] and anatase [20] surfaces. The water environment is not included [19,30], an acceptable approximation for studying trends in structurally similar systems [31]. The 1×4 reconstruction of anatase (001) is destabilized under electrochemical conditions and is also neglected [20]. The Gibbs free energy changes (ΔG) for the four OER steps are determined by combining DFT total energy and vibrational frequency calculations at $T = 0 \text{ K}$ with standard thermodynamic data for molecules in the gas and liquid phases. We further use the standard hydrogen electrode (SHE) as the reference potential [30], with the dependencies on $p\text{H}$ and U included as simple additional terms in ΔG [30]. Following Ref. [20], we take $p\text{H} = 0$ and $U = 1.93 \text{ V}$, which corresponds to an overpotential of 0.7 V , as found experimentally for rutile TiO_2 nanowires [32].

In Fig. 2 we compare our computed OER free-energy profiles for the heterostructures of Fig. 1(A) and on unsupported anatase (001), for which our results agree well with previous DFT studies [19,20]. For unsupported anatase (black dotted line) there is a thermodynamic barrier of 0.45 eV , which originates from the first deprotonation of the first adsorbed water molecule (step $1 \rightarrow 1'$). For negatively polarized $(\text{TiO}_2/\text{STO})_-$, the free-energy profile (blue line) is almost identical to that of unsupported TiO_2 , despite the large negative polarization (-0.8 C/m^2) of the STO substrate. By contrast, for positively polarized $(\text{TiO}_2/\text{STO})_+$ there are major differences (red line), especially for the $1 \rightarrow 1'$ step, whose ΔG changes from endothermic to strongly exothermic. As a result, the overall thermodynamic barrier is strongly reduced, from 0.45 eV on unsupported TiO_2 to $\sim 0.09 \text{ eV}$ on $(\text{TiO}_2/\text{STO})_+$. To test the robustness of this prediction, we determined ΔG for the key $1 \rightarrow 1'$ step using the DFT(GGA) + U approach, that is widely applied to transition metal oxides [33–35], including studies of the OER [36]. Using $U = 3 \text{ eV}$ for the Ti 3d states, a value that works well for both TiO_2 [33,34] and STO [35], we found no significant difference from the results in Fig. 2 (see Fig. S1 of the Supplemental Material [26]). We also examined the effect of the TiO_2 slab thickness and found that the $1 \rightarrow 1'$ step remains exothermic ($\Delta G = -0.6 \text{ eV}$ at the GGA level) when the thickness of the TiO_2 film is increased from four to eight layers.

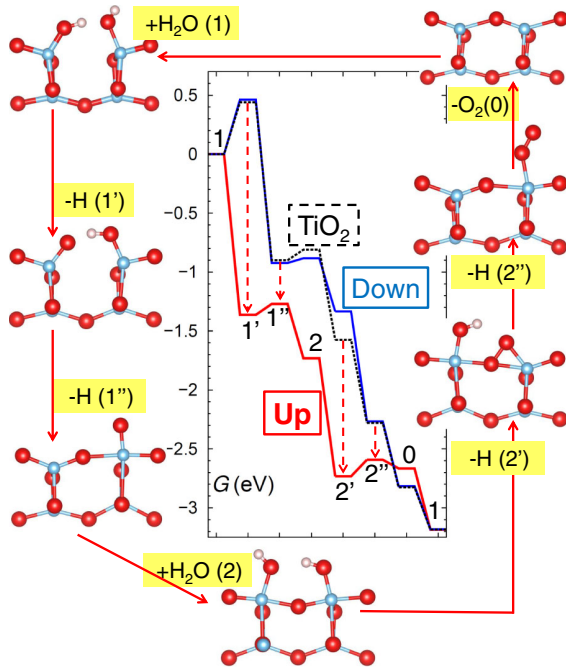


FIG. 2 (color online). OER free energy profile on unsupported TiO_2 (black), and on the positively (red) and negatively (blue) polarized TiO_2/STO of Fig. 1 at $\text{pH} = 0$ and $U = 1.93$ V vs SHE. Note that the free energy change in a full catalytic cycle (from 1 to 1) is -3.2 eV rather than $-2.8 (= 4.92 - 4 \times 1.93)$ eV, as expected with $U = 1.93$ V, due to the PBE overestimate of the $\text{O}_2(\text{g})$ binding energy. Atomic structures refer to the OER on $(\text{TiO}_2/\text{STO})_+$. The color code for the different atoms is as in Fig. 1. Vertical dashed red lines indicate the energy difference between unsupported TiO_2 and $(\text{TiO}_2/\text{STO})_+$ along the various OER steps.

To explain the results in Fig. 2, we computed the induced polarization of the anatase film, P_{TiO_2} , along the OER. P_{TiO_2} is small and negative for $(\text{TiO}_2/\text{STO})_-$ and pure TiO_2 alike (Fig. 3), whereas it is large and positive for $(\text{TiO}_2/\text{STO})_+$. The induced polarization can be converted to an induced surface charge ΔQ ($Q = A \times P, A =$ surface area of TiO_2). For $(\text{TiO}_2/\text{STO})_+$, ΔQ is $+0.72e$ after the first proton coupled electron transfer (PCET), which leaves an adsorbed hydroxyl bearing a negative charge, $\text{OH}^{-\alpha}$ ($1'$), and linearly increases to $+1.5e$ after the second PCET, which leaves an oxygen adatom $\text{O}^{-2\beta}$ ($1''$) ($0 \leq \alpha, \beta \leq 1$). These induced positive charges selectively stabilize the negatively charged adsorbates, eliminating the $1 \rightarrow 1'$ barrier. During the reaction cycle, P_{TiO_2} first reaches (and even slightly surpasses) the polarization, 0.8 C/m^2 , of the bottom STO layer, and then gradually decreases to 0.04 C/m^2 for the bare surface (0). The small P_{TiO_2} for the bare surface results from the presence of screening charges at the STO/TiO_2 interface, as shown by the layer resolved DOS (Fig. S2-1 [26]). Associated to the large polarization during the cycle there is a potential drop of ~ 1 eV inside the TiO_2 layers, as well as a large electric field of $\sim 0.1 \text{ eV/\AA}$ (see Figs. S2-2–S2-6 in the Supplemental Material [26]). In experiments, this dynamically induced field

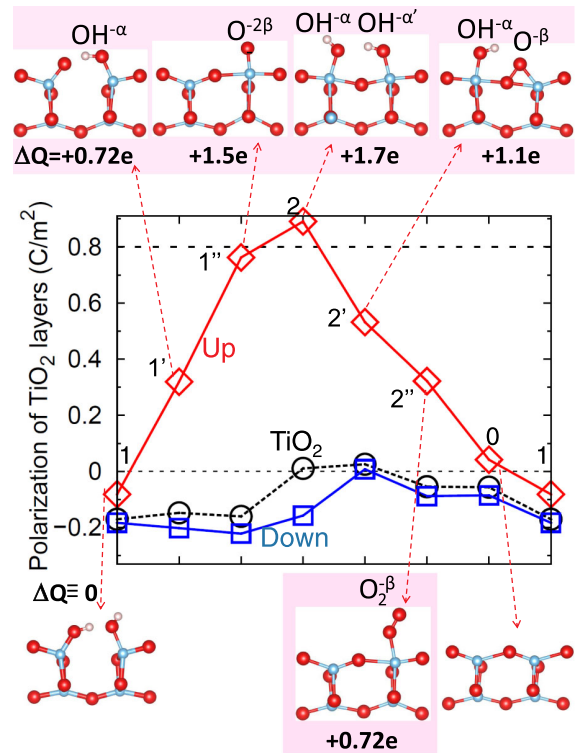


FIG. 3 (color online). Induced TiO_2 polarization during the OER on unsupported TiO_2 (black), and positively (red) and negatively (blue) polarized TiO_2/STO , as shown in Fig. 2. Dashed red arrows indicate the atomic structures of the intermediates on $(\text{TiO}_2/\text{STO})_+$. The horizontal line at $P_{\text{TiO}_2} = 0.8 \text{ C/m}^2$ indicates the magnitude of the polarization of the bottom STO layer in the heterostructures.

could help separating electrons and holes and boost the diffusion of the holes toward the TiO_2 surface during the intermediate steps of the reaction. Typical switching times of polar domain wall ($\sim \text{nm}$) in oxide films vary from nano- to subpicosecond [37,38]. The switching time of the relevant dipoles ($\sim \text{\AA}$) at the TiO_2 surface is expected to be much faster, so they can respond promptly to the changes in the charge of the adsorbed species during the reaction, whose characteristic times have a lower limit of ~ 1.5 ps [39].

Using strain to control the surface reactivity is an appealing possibility [40–42]. To examine the effect of strain on the reactivity of TiO_2/STO , we studied the OER on various strained $(\text{TiO}_2/\text{STO})_+$ heterostructures, with the STO polarization proportional to the strain [16]. Our results are reported in Fig. 4, where the strain is referred to anatase, so that a tensile strain of $+3.8\%$ is close to the computed equilibrium lattice parameter of STO. Configuration 2 (after adsorption of the second water molecule) is the most affected by epitaxial strain, with a free energy drop of almost 2 eV when the strain changes from $+3.8\%$ to -1% . This effect can be understood as follows. Under zero or compressive strain, the large positive STO polarization leads to large surface

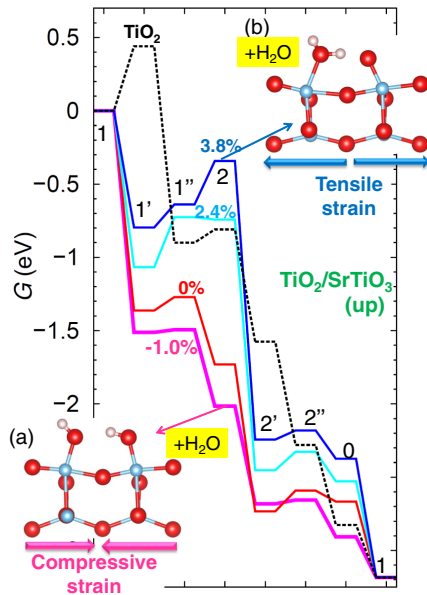


FIG. 4 (color online). Free energy profiles for the OER on strained $(\text{TiO}_2/\text{STO})_+$ heterostructures and on pure TiO_2 (black dotted line) at $p\text{H} = 0$ and $U = 1.93$ V vs SHE. The reported strain is measured relative to TiO_2 , so that a strain of 3.8% corresponds to the (theoretical) lattice constant of STO. The atomic structures represent water adsorbed on TiO_2/STO with 1% compressive (a) and 3.8% tensile (b) strain.

→ adsorbate charge transfers (Fig. 3). As a result, the oxygen adatom in configuration 1'' (before adsorption of the second water molecule) has a large negative charge, i.e. large proton affinity, and is thus able to deprotonate a newly adsorbed water molecule. Configuration 2 consists indeed of two adsorbed hydroxyls and is very stable. Conversely, tensile strain corresponds to small STO polarization, small surface → adsorbate charge transfers, and therefore small negative charge on the oxygen adatom in configuration 1''. When the second water molecule is adsorbed (configuration 2), the oxygen adatom is not able to deprotonate it, but can only form an H bond with it. The resulting configuration is not energetically favorable, however, likely because the oxygen adatom remains highly undercoordinated. In fact, this configuration is even less favorable than configuration 2 on pure TiO_2 or negatively polarized TiO_2/STO , where the oxygen adatom is essentially neutral and can thus bind to the twofold oxygen on the TiO_2 surface (see Ref. [20] and Fig. S2-4 [26]). To sum up, the results in Fig. 4 indicate that by combining strain with polarization it is possible to generate a pathway with strongly reduced thermodynamic barriers relative to unsupported TiO_2 .

In the results presented so far, the atomic positions of the bottom STO layer were fixed to those of strained bulk STO so as to mimic a thick ferroelectric STO layer (Fig. S3 in the Supplemental Material [26]). However, it is experimentally challenging to prepare thick coherent films with large

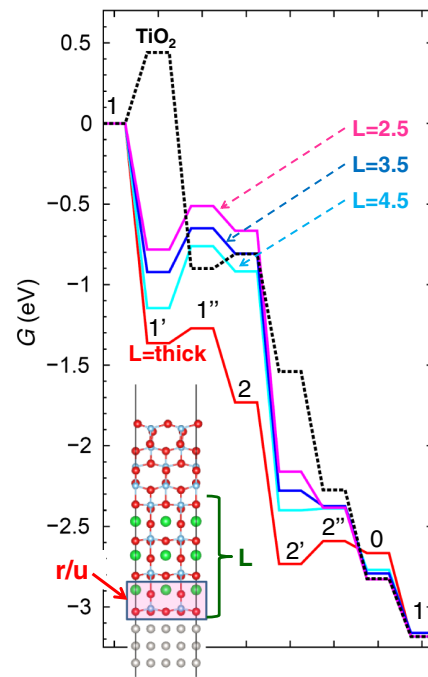


FIG. 5 (color online). Free energy profiles for the OER ($U = 1.93$ V vs SHE, $p\text{H} = 0$) on TiO_2/STO heterostructures formed by anatase on thin STO films of thickness $L = 4.5$ – 2.5 unit cells, epitaxially compressed to match the anatase lattice. The atomic coordinates in the STO film are fully relaxed. For comparison, also shown are two OER profiles already reported in Fig. 2, for pure TiO_2 (black dotted line) and the positively polarized TiO_2/STO heterostructure (red line) with a thick STO substrate. The heterostructure in the inset shows the STO layers which are either fully relaxed (r) or kept fixed (u) to represent a thin film or thick substrate, respectively.

epitaxial strains of 3%–4% [17], as used to obtain the profiles shown in Figs. 2 and 4. As an alternative possibility, we have considered thin STO films without any built-in polarization, epitaxially compressed to match the TiO_2 lattice. Figure 5 shows the OER profiles for TiO_2/STO heterostructures in which all atomic positions in the STO film ($L = 4.5$ – 2.5 unit-cell thick) are fully relaxed in order to represent a thin layer of high- k STO. Although there is no net polarization from STO initially, large positive polarizations (~ 0.5 C/m²) are induced in the TiO_2 layers during the intermediate steps of the reaction (Fig. S4 [26]), with a pattern qualitatively similar to that found for the thick STO substrate. Due to the smaller polarization of the thin STO substrate, however, in Fig. 5 small thermodynamic barriers remain, notably for the second deprotonation, $1 \rightarrow 1'$, step.

In conclusion, our study shows that the OER activity of heterostructures of TiO_2 on a polar substrate can be strongly enhanced relative to unsupported TiO_2 due to dynamical dipoles induced in response to the charge on the adsorbed species. By utilizing substrate polarization and strain as control parameters, these versatile structures hold

significant promise as new efficient catalysts for water splitting and other (photo)chemical reactions.

We thank Ye-Fei Li, Jia Chen, Kevin Garrity, Kieron Burke, Morrel H. Cohen, Karin Rabe, Raffaele Resta, and David Vanderbilt for helpful discussions. This work was supported by DOE-BES, Division of Chemical Sciences, Geosciences, and Biosciences under Grant No. DE-FG02-05ER15702. We acknowledge the use of computer resources at the TIGRESS high performance computer center of Princeton University, and at the center for Functional Nanomaterials, Brookhaven National Laboratory.

*Corresponding author.

leej@ornl.gov

Present address: Materials Science and Technology Division, Oak Ridge National Laboratory, Oak Ridge, TN 37831, USA.

- [1] A. L. Linsebigler, G. Lu, and J. T. Yates, Jr., *Chem. Rev.* **95**, 735 (1995).
- [2] A. Fujishima, X. T. Zhang, and D. A. Tryk, *Surf. Sci. Rep.* **63**, 515 (2008).
- [3] M. A. Henderson, *Surf. Sci. Rep.* **66**, 185 (2011).
- [4] R. Asahi, T. Morikawa, T. Ohwaki, K. Aoki, and Y. Taga, *Science* **293**, 269 (2001).
- [5] H. G. Yang, C. H. Sun, S. Z. Qiao, J. Zou, G. Liu, S. C. Smith, H. M. Cheng, and G. Q. Lu, *Nature (London)* **453**, 638 (2008).
- [6] S. V. Kalinin, D. A. Bonnell, T. Alvarez, X. Lei, Z. Hu, J. H. Ferris, Q. Zhang, and S. Dunn, *Nano Lett.* **2**, 589 (2002).
- [7] J. L. Giocondi and G. S. Rohrer, *Chem. Mater.* **13**, 241 (2001).
- [8] D. Tiwari and S. Dunn, *J. Mater. Sci.* **44**, 5063 (2009).
- [9] J. Shin, V. B. Nascimento, G. Geneste, J. Rundgren, E. W. Plummer, B. Dkhil, S. V. Kalinin, and A. P. Baddorf, *Nano Lett.* **9**, 3720 (2009).
- [10] S. V. Levchenko and A. M. Rappe, *Phys. Rev. Lett.* **100** (2008).
- [11] D. Cappus, M. Haßel, E. Neuhaus, M. Heber, F. Rohr, and H. J. Freund, *Surf. Sci.* **337**, 268 (1995).
- [12] N. V. Burbure, P. A. Salvador, and G. S. Rohrer, *J. Am. Ceram. Soc.* **89**, 2943 (2006).
- [13] L. Li, G. S. Rohrer, and P. A. Salvador, *J. Am. Ceram. Soc.* **95**, 1414 (2012).
- [14] Y. Zhang, A. M. Schultz, P. A. Salvador, and G. S. Rohrer, *J. Mater. Chem.* **21**, 4168 (2011).
- [15] L. Kavan, M. Gratzel, S. E. Gilbert, C. Klemenz, and H. J. Scheel, *J. Am. Chem. Soc.* **118**, 6716 (1996).
- [16] A. Antons, J. B. Neaton, K. M. Rabe, and D. Vanderbilt, *Phys. Rev. B* **71**, 024102 (2005).
- [17] D. G. Schlom, L. Q. Chen, C. B. Eom, K. M. Rabe, S. K. Streiffer, and J. M. Triscone, in *Annual Review of Materials Research* (Annual Reviews, Palo Alto, 2007), Vol. 37, p. 589.
- [18] S. A. Chambers, *Adv. Mater.* **22**, 219 (2010).
- [19] A. Valdés, Z. W. Qu, G. J. Kroes, J. Rossmeisl, and J. K. Nørskov, *J. Phys. Chem. C* **112**, 9872 (2008).
- [20] Y.-F. Li, Z.-P. Liu, L. Liu, and W. Gao, *J. Am. Chem. Soc.* **132**, 13008 (2010).
- [21] J. P. Perdew, K. Burke, and M. Ernzerhof, *Phys. Rev. Lett.* **77** (1996).
- [22] P. Giannozzi *et al.*, *J. Phys. Condens. Matter* **21**, 395502 (2009).
- [23] V. I. Anisimov, J. Zaanen, and O. K. Andersen, *Phys. Rev. B* **44**, 943 (1991).
- [24] A. M. Kolpak, I. Grinberg, and A. M. Rappe, *Phys. Rev. Lett.* **98** (2007).
- [25] K. Garrity, A. Kakekhani, A. Kolpak, and S. Ismail-Beigi, *Phys. Rev. B* **88**, 045401 (2013).
- [26] See Supplemental Material at <http://link.aps.org/supplemental/10.1103/PhysRevLett.112.196102> for the method of calculation of the induced polarization in TiO₂, comparison between GGA and GGA + *U* calculation of the free energy for the first OER deprotonation step, layer resolved density of states along the OER, dependence of the OER free energy profile, and induced polarization on the number of layers in the STO substrate.
- [27] D. D. Fong *et al.*, *Phys. Rev. Lett.* **96**, 127601 (2006).
- [28] R. D. King-Smith and D. Vanderbilt, *Phys. Rev. B* **47**, 1651 (1993).
- [29] R. J. Gonzalez, R. Zallen, and H. Berger, *Phys. Rev. B* **55**, 7014 (1997).
- [30] J. Rossmeisl, Z. W. Qu, H. Zhu, G. J. Kroes, and J. K. Nørskov, *J. Electroanal. Chem.* **607**, 83 (2007).
- [31] I. C. Man *et al.*, *Chem. Cat. Chem.* **3**, 1159 (2011).
- [32] B. Liu, H. M. Chen, C. Liu, S. C. Andrews, C. Hahn, and P. Yang, *J. Am. Chem. Soc.* **135**, 9995 (2013).
- [33] E. Finazzi, C. Di Valentin, G. Pacchioni, and A. Selloni, *J. Chem. Phys.* **129**, 154113 (2008).
- [34] Z. Hu and H. Metiu, *J. Phys. Chem. C* **115**, 5841 (2011).
- [35] D. Doennig, W. E. Pickett, and R. Pentcheva, *Phys. Rev. Lett.* **111**, 126804 (2013).
- [36] M. García-Mota, M. Bajdich, V. Viswanathan, A. Vojvodic, A. T. Bell, and J. K. Nørskov, *J. Phys. Chem. C* **116**, 21077 (2012).
- [37] J. F. Scott, *Ferroelectric Memories* (Springer, New York, 2000).
- [38] J. Li, B. Nagaraj, H. Liang, W. Cao, C. H. Lee, and R. Ramesh, *Appl. Phys. Lett.* **84**, 1174 (2004).
- [39] A. V. Akimov, J. T. Muckerman, and O. V. Prezhdo, *J. Am. Chem. Soc.* **135**, 8682 (2013).
- [40] M. Mavrikakis, B. Hammer, and J. K. Nørskov, *Phys. Rev. Lett.* **81**, 2819 (1998).
- [41] A. Kushima, S. Yip, and B. Yildiz, *Phys. Rev. B* **82**, 115435 (2010).
- [42] P. Strasser *et al.*, *Nat. Chem.* **2**, 454 (2010).